Green Chemistry

PAPER

View Article Online
View Journal | View Issue

Cite this: *Green Chem.*, 2019, **21**, 1517

Electrodeposition of indium from the ionic liquid trihexyl(tetradecyl)phosphonium chloride†

Clio Deferm, [a,b] João C. Malaquias,[c] Bieke Onghena, [a] Dipanjan Banerjee, [d] Jan Luyten,[b] Harald Oosterhof,[b] Jan Fransaer [c] and Koen Binnemans *[a]

Received 29th October 2018,
Accepted 23rd January 2019

DOI: 10.1039/c8gc03389g

rsc.li/greenchem

The electrochemical behavior of indium in the ionic liquid trihexyl(tetradecyl)phosphonium chloride (Cyphos IL 101) was studied. Cyphos IL 101 first had to be purified, as the impurities present in commercial Cyphos IL 101 interfered with the electrochemical measurements. Electrochemical deposition of indium metal from this electrolyte occurs without hydrogen evolution, increasing the cathodic current efficiency compared to deposition from water and avoiding porosity within the deposited metal. Indium(III) is the most stable oxidation state in the ionic liquid. This ion is reduced in two steps, first from indium(III) to indium(I) and subsequently to indium(0). The high thermal stability of Cyphos IL 101 allowed the electrodeposition of indium at 120 °C and 180 °C. At 180 °C indium was deposited as liquid indium which allows for the easy separation of the indium and the possibility to design a continuous electrowinning process. On molybdenum, indium deposits as liquid droplets even below the melting point of indium. This was explained by the combination of melting point depression and undercooling. The possibility to separate indium from iron and zinc by electrodeposition was tested. It is possible to separate indium from zinc by electrodeposition, but iron deposits together with indium.

Introduction

Indium is important for the electronics industry. Indium-containing semiconductors, such as indium phosphide (InP), indium selenide (InSe), copper indium selenide (CIS), copper indium gallium selenide (CIGS), indium arsenide (InAs), indium gallium phosphide (InGaP), and indium tin oxide (ITO), are essential for components of many electronic and optoelectronic devices (*e.g.* detectors, lasers, photovoltaic devices and light-emitting diodes).[1,2] Indium also finds application in low-temperature alloy solders.[1,2] Electrochemical deposition is one of many different fabrication techniques for these materials, next to closed-space sublimation,[3] metal organic chemical vapor deposition,[4] co-evaporation[5] and molecular beam epitaxy.[6] The advantages of electrodeposition over the other techniques are: lower required temperatures, the possibility to work at ambient pressure with a high deposition rate, easily controllable and low-cost equipment and inexpensive precursors.[7,8] Electrochemical deposition of indium is also of importance for the purification of indium, as high-purity indium is often required as a starting material for the above-mentioned applications. Electrowinning of indium can be an essential step in the recovery of indium from primary and secondary sources.[9–14]

Electrochemical deposition of indium from aqueous electrolytes has been extensively described in the literature.[12,14,15] It is often complicated due to the simultaneous formation of hydrogen gas, which decreases the electrodeposition efficiency and can cause dendritic growth, pinholes and hydrogen embrittlement.[16,17] The use of aprotic ionic liquid electrolytes can circumvent the complications associated with hydrogen evolution. Moreover, ionic liquids exhibit a good electrical conductivity, low vapor pressure, good thermal stability and a wide electrochemical window, allowing deposition of metals that cannot be deposited from water, *e.g.* aluminum.[18–21]

Ionic liquids are solvents that consist entirely of ions. Two main families of ionic liquids are commonly used for electrochemical deposition purposes: first-generation chloroaluminate ionic liquids, and second-generation "air- and water-stable" ionic liquids with hydrophobic anions, such as tetrafluoroborate, hexafluorophosphate, trifluoromethanesulfonate or bis(trifluoromethylsulfonyl)imide. Until now, numerous

[a]*KU Leuven, Department of Chemistry, Celestijnenlaan 200F, bus 2404, B-3001 Heverlee, Belgium. E-mail: Koen.Binnemans@kuleuven.be*
[b]*Umicore, Group Research & Development, Competence Area Recycling and Extraction Technologies, Watertorenstraat 33, B-2250 Olen, Belgium*
[c]*KU Leuven, Department of Materials Engineering, Kasteelpark Arenberg 44, bus 2450, B-3001 Heverlee, Belgium*
[d]*Dutch-Belgian Beamline (DUBBLE), ESRF – The European Synchrotron, CS 40220, 38043 Grenoble Cedex 9, France*

†Electronic supplementary information (ESI) available: Experimental, first cycle CVs, diffusion coefficient determination, pictures of flasks with indium electrolyte, SEM images, EDS spectra, a DSC trace and additional EXAFS functions and the corresponding FT. See DOI: 10.1039/c8gc03389g

examples of the use of first-generation ionic liquids for the electrochemical deposition of single metals and alloys, including indium, have been reported.[22–24] The disadvantage of the chloroaluminate ionic liquids is that they are very prone to hydrolysis, so that they must be handled in a glovebox. The replacement of the moisture-sensitive anions in the first-generation ionic liquids has led to the design of air- and water-stable second-generation ionic liquids.[25] Moreover, a new class of ionic liquid analogues, deep-eutectic solvents, are emerging as electrolytes for metal electrodeposition.[26] Until now, only a small number of papers report on the electrodeposition of indium or indium alloys from second-generation ionic liquids or deep-eutectic solvents.[27–38]

High-temperature electrometallurgy using a liquid cathode is used in industry to recover or refine metals, such as aluminum *via* the Hall–Héroult process.[39] Electrodeposition using a liquid cathode has also been studied for the electrowinning and electrorefining of the rare earths, actinides and titanium.[40–45] The use of a liquid cathode offers several advantages: (1) easy separation of electrolysis products due to the large density difference between the electrolyte and the liquid cathode, (2) a constant electrode surface area that permits stable values for the process parameters, (3) irregular crystal growth is avoided, so lower operating voltages are required due to the shorter distance between cathode and anode, (4) easier coalescence of microdrops and metallic fog and (5) the possibility to design a continuous process.[40,41,46] High-temperature electrowinning of indium has been reported for molten salts electrolytes, but to the best of our knowledge, there is no study regarding indium electrowinning from ionic liquids at elevated temperatures.[47–50] The use of ionic liquids for electrowinning at temperatures above the melting point of indium can circumvent the complications associated with hydrogen evolution and can offer at the same time the advantages accompanied with the use of a liquid cathode.

In this paper, the electrochemical behavior of indium in the ionic liquid trihexyl(tetradecyl)phosphonium chloride (Cyphos IL 101) is described. The electrodeposition of indium above its melting point is reported. The morphology of the indium deposits was examined alongside the separation of indium from zinc and iron *via* electrodeposition. The high-temperature electrowinning of liquid indium allows for an easy separation of the indium and the possibility to design a continuous electrowinning process.

Results and discussion

Electrochemical study in commercial Cyphos IL 101

In a first step, the electrochemical window (EW) of commercial trihexyl(tetradecyl)phosphonium chloride, Cyphos IL 101, was determined. Fig. 1 shows the cyclic voltammograms (CVs) of commercial Cyphos IL 101 recorded on a Pt or Mo electrode at 120 °C and 180 °C at a scan rate of 20 mV s^{-1}. The limiting potentials and the corresponding EW for different experimental conditions are shown in Table 1. The EW are narrow: between 0.73 V and 1.31 V *vs.* Fc^+/Fc. Ionic liquids generally have wide electrochemical windows, often exceeding 4.00 V.[51–53] Furthermore, the trihexyl(tetradecyl)phosphonium cation is reported to have a very high resistance to reduction.[51,54] Commercial Cyphos IL 101 typically assays >97% trihexyl(tetradecyl)phosphonium chloride. However, the product also contains small amounts of tetradecane isomers, dihexyl phosphine (PR_2H), HCl and trihexylphosphonium hydrochloride ($[PR_3H]Cl$).[55–58] It has been shown that the presence of electroactive impurities in ionic liquids can cause an apparent narrowing of the true EW.[59,60] The first reductive wave in the forward cycle is possibly a consequence of the reduction of impurities. The narrowing of the EW makes the use of high-purity ionic liquids in electrochemical applications necessary.[53,61] Therefore, the commercial

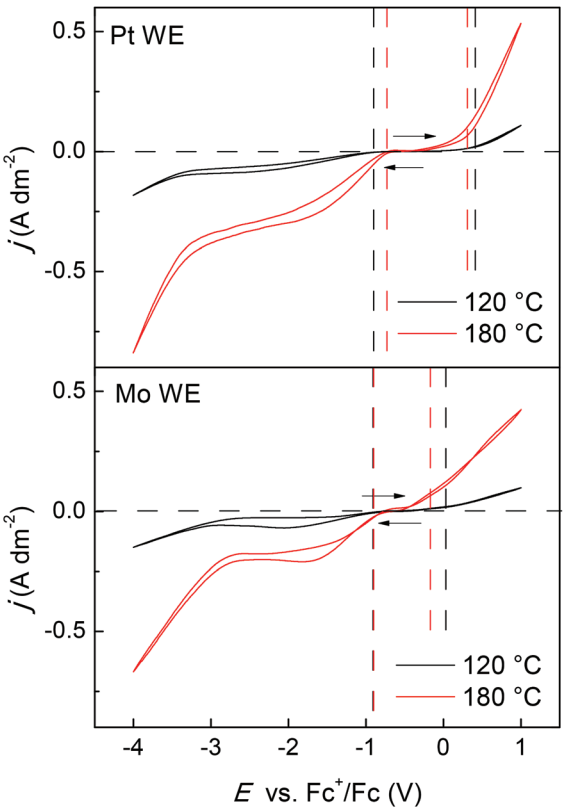

Fig. 1 CVs (2nd cycle) of commercial Cyphos IL 101 recorded on a Pt and Mo working electrode at 120 °C and 180 °C. Scans were recorded at v_{scan} = 20 mV s^{-1}. CVs (1st cycle) are shown in ESI, Fig. S1.†

Table 1 Limiting potentials and corresponding electrochemical window (EW) of commercial Cyphos IL 101 recorded on different working electrodes (WE) and temperatures

WE	Temperature (°C)	Cathodic limit *vs.* Fc^+/Fc (V)	Anodic limit *vs.* Fc^+/Fc (V)	EW (V)
Pt	120	−0.90	0.41	1.31
	180	−0.73	0.31	1.04
Mo	120	−0.91	0.03	0.94
	180	−0.90	−0.17	0.73

Cyphos IL 101 was thus purified prior to determining its true EW according to a literature method as described in the ESI.† [55]

Electrochemical stability of purified Cyphos IL 101

Fig. 2 shows the CV of purified Cyphos IL 101 recorded on a Pt or Mo electrode at 120 °C and 180 °C at a scan rate of 20 mV s^{-1}. The limiting potentials and the corresponding EW according to the experimental conditions are shown in Table 2. By removing the impurities present in the commercial Cyphos IL 101, the true EW of the electrolyte becomes observable. This true EW is about 1.5 times wider than the EW observed in the as-received commercial product. It is suggested that the limiting potentials correspond to the cathodic reduction of the phosphonium cation and the anodic oxidation of the chloride anion. When comparing the CV of the commercial Cyphos IL 101 (Fig. 1) to the purified Cyphos IL 101 (Fig. 2), a clear improvement was observed: for the purified Cyphos IL 101, the cathodic part of the window shows no reactions besides the decomposition of Cyphos IL 101 itself. Also, the decomposition of commercial Cyphos IL 101 is starting at a more negative potential than that of purified Cyphos IL 101. The impurities that are reduced during the first reductive wave are probably deposited on the electrode surface, thereby decreasing its active surface area.

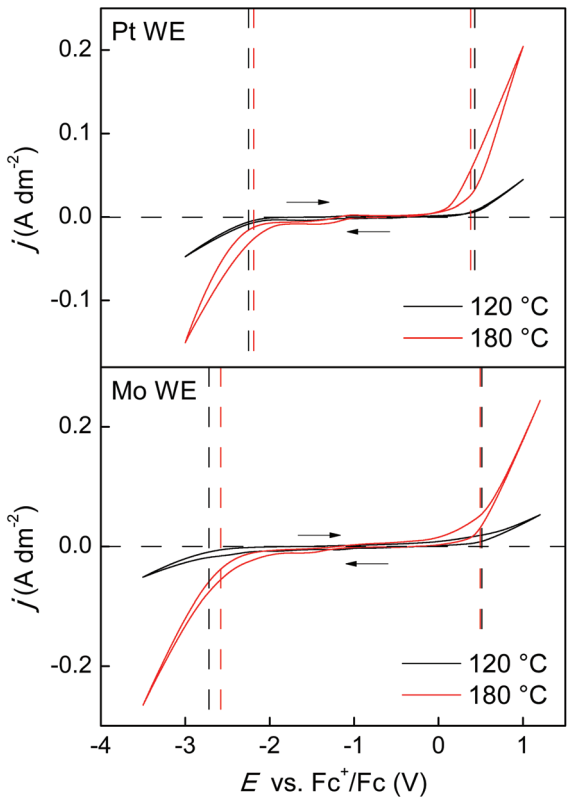

Fig. 2 CVs (2nd cycle) of purified Cyphos IL 101 recorded on a Pt working electrode and Mo working electrode (WE) at 120 °C and 180 °C. Scans were recorded at v_{scan} = 20 mV s^{-1}. CVs (1st cycle) are shown in ESI, Fig. S2.†

Table 2 Limiting potentials and corresponding electrochemical window (EW) of purified Cyphos IL 101 recorded on different working electrodes (WE) and temperatures

WE	Temperature (°C)	Cathodic limit *vs.* Fc^+/Fc (V)	Anodic limit *vs.* Fc^+/Fc (V)	EW (V)
Pt	120	−2.25	0.43	2.68
	180	−2.19	0.38	2.57
Mo	120	−2.72	0.51	3.23
	180	−2.58	0.49	3.07

In order to find an explanation for the narrowing of the electrochemical window of commercial Cyphos IL 101 by the reductive wave (Fig. 1), several known impurities of commercial Cyphos IL 101 were added separately to the purified Cyphos IL 101: 3 wt% of Cyanex 923 (mixture of four trialkylphosphine oxides)[62] or 3 wt% of Cytop 360 (trihexylphosphine). Fig. S3 in the ESI† compares the CVs of purified Cyphos IL 101, commercial Cyphos IL 101 and purified Cyphos IL 101 containing 3 wt% of Cyanex 923 or 3 wt% of Cytop 360, recorded on a platinum electrode at 120 °C and 180 °C and a scan rate of 20 mV s^{-1}. When comparing the CVs, it is clear that the reduction wave in the CV of commercial Cyphos IL 101 cannot be attributed to phosphine oxide or trihexylphosphine impurities. No additional reduction wave, besides the decomposition of the phosphonium cation, was observed in the CV of purified Cyphos IL 101 containing 3 wt% of Cyanex 923 or Cytop 360. Vaughan and Dreisinger postulated that the additional reduction wave is attributed to the evolution of hydrogen from the $[PR_3H]Cl$ and HCl impurities.[63] Since a difference in hydrogen overpotential is expected between molybdenum and platinum, the potential at which hydrogen gas becomes possible, depends on the metal used as working electrode. Cyphos IL 101 is prepared in industry *via* a quaternization reaction of trihexylphosphine (Cytop 360) with 1-chlorotetradecane (nucleophilic substitution S_N2).[55,57] Several impurities present in Cytop 360 can be quaternized as well, ending up as impurities in Cyphos IL 101. The reduction of these quaternized impurities will only be seen in the CVs of commercial Cyphos IL 101 and are probably causing the additional reduction wave.

Electrochemical study of indium in purified Cyphos IL 101

The electrochemical behavior of indium in the purified Cyphos IL 101 was studied. Fig. 3 shows the CVs of the purified ionic liquid loaded with 10 mM of indium(III) recorded on a platinum electrode at 120 °C and 180 °C at a scan rate of 20 mV s^{-1}. The CVs show a cathodic wave in the forward cycle starting at E = −2.15 V *vs.* Fc^+/Fc at 120 °C and E = −1.80 V *vs.* Fc^+/Fc at 180 °C, corresponding to the reduction of indium(III). There are only small differences (about 0.1 V) in the standard reduction potentials (E_0) of the redox couple In^{3+}/In, In^{3+}/In^+ and In^{3+}/In^{2+}.[64] It is possible that the cathodic wave includes the following reactions.

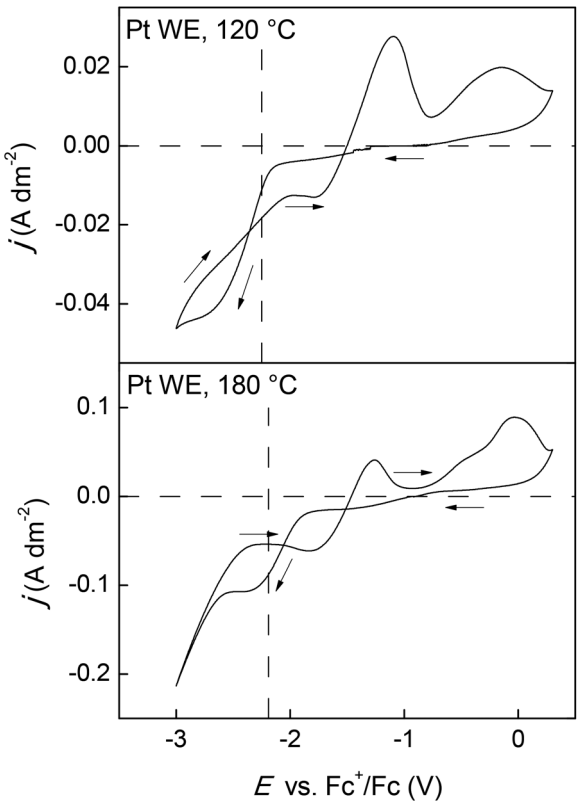

Fig. 3 CVs (2nd cycle) of purified Cyphos IL 101 loaded with 10 mM of indium(III) on a Pt working electrode (WE) at 120 °C and 180 °C. Scans were recorded at v_{scan} = 20 mV s^{-1}. CVs (1st cycle) are shown in ESI, Fig. S4.†

$$In^{3+} + 3e^- \rightleftharpoons In \quad E_0 = -0.3382\ V \quad (1)$$

$$In^{3+} + 2e^- \rightleftharpoons In^+ \quad E_0 = -0.443\ V \quad (2)$$

$$In^{3+} + e^- \rightleftharpoons In^{2+} \quad E_0 = -0.49\ V \quad (3)$$

$$In^{2+} + e^- \rightleftharpoons In^+ \quad E_0 = -0.40\ V \quad (4)$$

The existence of indium(I) species in chloroindate(III) ionic liquid system, including the $InCl_3$–Cyphos IL 101 system, has already been demonstrated.[33,65] While the existence of indium(II) species in ionic liquids is still unclear. Based on this information, it is assumed that the In^{3+}/In^+ reduction takes place, although we do not exclude that both the In^{3+}/In^+ reduction and In^{3+}/In^{2+} reduction are at play. A nucleation loop was observed, indicating a hindered growth on the electrode surface. This behavior is typical for processes which require a large overpotential to form a deposit. Also, a cathodic peak was observed in the backward scan, possibly resulting from the reduction of indium(I), created in the forward scan, to indium metal. At approximately −1.11 V *vs.* Fc^+/Fc at 120 °C and −1.26 V *vs.* Fc^+/Fc at 180 °C, an anodic peak was observed in the CVs which implies the stripping of the metallic indium deposited in the forward scan. The second oxidation peak in the CV starting at −0.75 V *vs.* Fc^+/Fc at 120 °C and −0.85 V *vs.* Fc^+/Fc at 180 °C is attributed to the stripping of various indium–platinum alloys.[66] At 180 °C, the broadness of this peak is likely due to the formation of more than one type of intermetallic compound. The fact that the stripping peak of the alloy is higher than that of pure indium indicates that the formation of intermetallics occurs rapidly and extensively, possibly due to the elevated temperature. The formation of indium–platinum alloys makes platinum less suitable as a WE for the recovery of pure indium.

The electrochemical behavior of indium in the purified Cyphos IL 101 was also studied on a molybdenum working electrode, as it does not alloy with indium.[67] Fig. 4 shows the CVs of the purified ionic liquid loaded with changing amounts of indium(III) (10, 20, 30, 40 and 50 mM) recorded at 120 °C and 180 °C and at a scan rate of 20 mV s^{-1}. Because a clear difference was observed between the first and second cycle at 120 °C, the first cycle was shown instead of the second one. In the previous CVs, the second cycle was identical to the first one. At 120 °C, the forward scan shows a cathodic peak between −1.35 V *vs.* Fc^+/Fc and −1.75 V *vs.* Fc^+/Fc probably corresponding to the reduction of indium(III) to indium(I). This peak is most outspoken at an indium concentration of 30 mM.

At higher or lower indium concentrations, it is difficult to distinguish this peak. At −2.00 V *vs.* Fc^+/Fc, indium(I) is

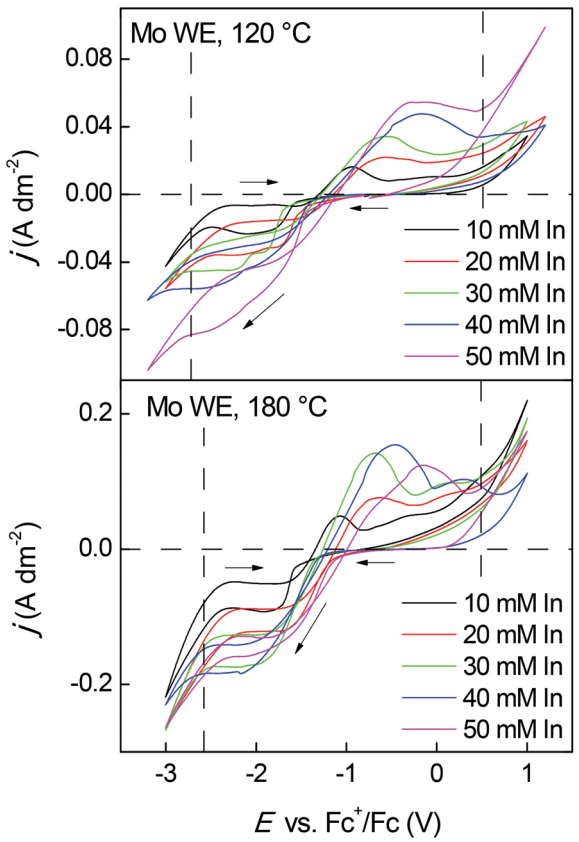

Fig. 4 CVs of purified Cyphos IL 101 loaded with 10, 20, 30, 40 and 50 mM of indium(III) on a Mo working electrode (WE) at 120 °C (1st cycle) and 180 °C (2st cycle). Scans were recorded at v_{scan} = 20 mV s^{-1}. A new WE was used for each measurement. CVs (1st cycle) at 180 °C are shown in ESI, Fig. S5.†

further reduced to indium metal, which can be observed from the presence of a nucleation loop. In the backward scan, two anodic peaks are detected. Probably the first anodic peak corresponds to the stripping of indium by electrochemical reaction of indium(0) to indium(I), while the second anodic peak is related to the oxidation of indium(I) to indium(III). Contrary to the CVs at 120 °C, the CVs at 180 °C show only one reduction peak. The cathodic peak that is located between −1.35 V *vs.* Fc^+/Fc and −1.50 V *vs.* Fc^+/Fc probably involves the two-step reduction of indium(III), going from indium(III) to indium(I) and finally to indium(0). Two anodic peaks are detected in the backward scan probably corresponding to the stripping of indium to indium(I) and the oxidation of indium (I) to indium(III). Fig. 5 shows a CV of purified Cyphos IL 101 loaded with 30 mM of indium(III) at 120 °C with three consecutive cycles. The forward scan of the first cycle clearly shows a two-step reduction process, which seems to evolve into a one-step reduction process with increasing consecutive cycle. After each experiment, a grey indium metal layer was still present on the molybdenum working electrode, indicating incomplete indium stripping. The nucleation loop in the first cycle is also considerably bigger than in the second and third cycle. Since it is thermodynamically more favorable to deposit indium on indium, the reduction of indium(III) to indium metal is favored above the two-step reduction process.

Besides varying the indium(III) concentration in the electrolyte, the scan rate was also varied to investigate the reversibility of the electrochemical processes. Fig. S6† shows the CVs of purified Cyphos IL 101 loaded with 30 mM of indium(III) at 120 °C and 180 °C with various scan rates (15, 20, 25, 50, 100 mV s^{-1}). The CVs at 120 °C represent the 1st cycle and a new WE was used for every measurement. The anodic and cathodic peak potentials, E_{pa} and E_{pc}, are dependent on the scan rate. As the scan rate increases, the separation between the anodic and cathodic peaks, $\Delta E_p = E_{pa} - E_{pc}$, becomes greater. This is characteristic for an irreversible or quasi-reversible system.[68]

To investigate the involvement of indium(I) or even indium(II) in the reduction process of indium(III) and oxidation process of indium metal in Cyphos IL 101, 30 mM of indium(I) chloride or 30 mM of indium(II) chloride was added to the purified electrolyte. After addition of indium(I) chloride or indium(II) chloride to the electrolyte, an immediate color change to silvery-grey was observed followed by particle coalescence resulting in the formation of a solid grey-silvery material, probably indium metal. The ionic liquid containing 30 mM of indium(II) also turned cloudy (Fig. S7†). It is hence likely that neither In(I) nor In(II) are stable in Cyphos IL 101 and that (complete or partial) disproportionation of indium(I) (eqn (5)) and indium(II) (eqn (6)) takes place:

$$3\mathrm{In(I)} \rightleftharpoons 2\mathrm{In}(0) + \mathrm{In(III)} \quad (5)$$

$$3\mathrm{In(II)} \rightleftharpoons \mathrm{In}(0) + 2\mathrm{In(III)} \quad (6)$$

As stated before, we do not exclude the existence of indium(II), but the formation of indium(I) in Cyphos IL 101 has already been demonstrated.[65] The disproportionation behavior of indium(I) can explain the appearance of a two-step reduction process in the first cycle on molybdenum evolving into a one-step reduction process with an increasing number of cycles. It was already established that the disproportionation of indium(I) is very fast in Cyphos IL 101.[65] It is possible that the disproportionation is hindered in the first cycle because a second phase (indium metal) must be formed in the electrolyte. In the second cycle, indium metal is already present on the electrode due to an incomplete stripping, facilitating the disproportionation reaction.

Fig. 6 shows the CVs of purified Cyphos IL 101 containing 30 mM of indium(I), 30 mM of indium(II) or 30 mM of indium(III) recorded on a molybdenum electrode at 120 °C and 180 °C at a scan rate of 20 mV s^{-1}. When comparing the CVs at 120 °C, it was noticed that the potential where the reduction current for indium(I) to indium(0) starts, in the indium(III)-containing electrolyte, coincides with the potential where the reduction starts of the indium present in the initial indium(I) and indium(II)-containing electrolytes. Although disproportionation of indium(I) or indium(II) takes place in these electrolytes forming indium(III) and indium metal, the CVs suggest that a certain concentration of indium(I) is in equilibrium with an indium(III) solution. The reduction wave starting at approximately −1.00 V *vs.* Fc^+/Fc in the forward cycle of the CVs is attributed to the reduction of indium(I) to indium(0). It is to be expected based on the standard reduction potentials of indium, that this reaction will take place at less negative potentials (eqn (7)) than the reduction of indium(III) to indium(0) (eqn (1)) or of indium(III) to indium(I) (eqn (2)).[64]

$$\mathrm{In^+ + e^- \rightleftharpoons In} \quad E_0 = -0.14\ \mathrm{V} \quad (7)$$

$$\mathrm{In^{2+} + e^- \rightleftharpoons In^+} \quad E_0 = -0.40\ \mathrm{V} \quad (8)$$

At 180 °C, a clear difference in the CVs was observed. The reduction wave in the indium(III)-containing electrolyte no longer coincides with the reduction wave in the initial indium(I)- and indium(II)-containing electrolytes. The cathodic peak, in the indium(III)-containing electrolyte, starting between

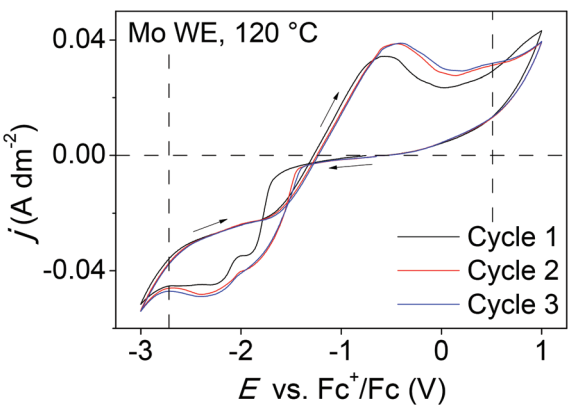

Fig. 5 CVs (three consecutive cycles) of purified Cyphos IL 101 loaded with 30 mM of indium(III) on a Mo working electrode (WE) at 120 °C. Scans were recorded at v_{scan} = 20 mV s^{-1}.

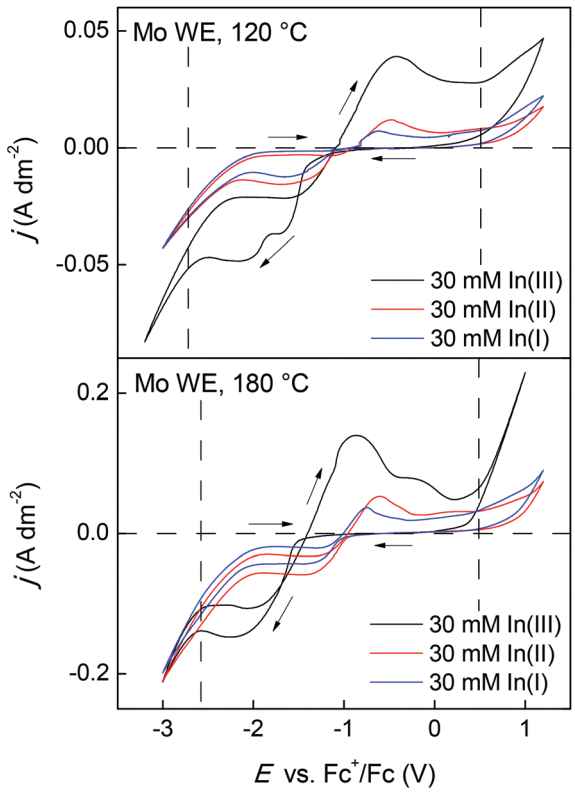

Fig. 6 CVs of purified Cyphos IL 101 loaded with 30 mM of indium(I), indium(II) or indium(III) on a Mo working electrode (WE) at 120 °C (1st cycle) and 180 °C (2nd cycle). Scans were recorded at v_{scan} = 20 mV s^{-1}. CVs (1st cycle) at 180 °C are shown in ESI, Fig. S8.†

−1.35 V *vs.* Fc^+/Fc and −1.50 V *vs.* Fc^+/Fc, probably involves the reduction of indium(III) to indium(I) and subsequently to indium metal while the cathodic peak starting at −1.00 V *vs.* Fc^+/Fc, in the indium(I)- and indium(II)-containing electrolytes, can be attributed to the reduction of indium(I) or indium(II) to indium (0). It is possible that the exchange current density for the indium(I) to indium(0) reduction is not high enough at 120 °C to observe a reduction wave in the CV of the initial indium(I)- and indium(II)-containing electrolytes. At 180 °C, the exchange current density is high enough to create a visible reduction wave.

To get a better insight in the cathodic reactions that take place, the potentiostat was coupled to an electrochemical quartz crystal microbalance (EQCM). A CV of the blank electrolyte with EQCM analysis was measured first as a reference situation and to determine if the reduction or oxidation of impurities leads to a change in mass on the electrode. The mass change of the quartz crystals is correlated to the frequency change using the Sauerbrey equation:

$$\Delta m = -C_f \Delta f \quad (9)$$

where Δf (Hz) is the change in the resonance frequency of the crystal (working electrode) due to the change in mass Δm (g cm^{-2}) of the crystal; C_f (g Hz^{-1} cm^{-2}) is the calibration constant. Fig. S9† shows the CV of purified Cyphos IL 101 with EQCM analysis. The CV was recorded at 120 °C on a Pt electrode with a scan rate of 2 mV s^{-1}. Since no significant shift in frequency was recorded from 0.50 V *vs.* Fc^+/Fc to −1.50 V *vs.* Fc^+/Fc in the forward or backward cycle, it can be assumed that the reduction and oxidation of impurities is not accompanied by a mass change. Also no significant mass change was observed between −1.50 V *vs.* Fc^+/Fc to −3.00 V *vs.* Fc^+/Fc together with the cathodic decomposition of the ionic liquid, indicating that it is not accompanied with the deposition of cathodic decomposition products or the formation of a solid compound on the WE. In the backward cycle, a high loss of mass was observed at the potential where anodic decomposition of the ionic liquid takes place. The formed chlorine gas reacted with the platinum WE forming platinum chloride that dissolves in the ionic liquid.

Fig. 7 shows the CV of purified Cyphos IL 101 loaded with 50 mM of indium(III) with EQCM analysis. The CV was recorded at 120 °C on a Pt electrode with a scan rate of 2 mV s^{-1}. A significant decrease in frequency was observed starting from −1.53 V *vs.* Fc^+/Fc in the forward cycle to −0.81 V *vs.* Fc^+/Fc in the backward cycle, indicating that deposition of indium(0) takes place. Although a noteworthy negative current starting from −0.77 V *vs.* Fc^+/Fc is observed in the forward cycle of the CV, it is not accompanied by a significant frequency change. This indicates the presence of a second reduction process without deposition starting at −0.77 V *vs.* Fc^+/Fc, most probably the reduction of indium(III) to indium(I). The reduction of indium(I) to indium(0) is presumably also included in the cathodic wave starting from −1.53 V *vs.* Fc^+/Fc. From −0.81 V *vs.* Fc^+/Fc to 0.83 V *vs.* Fc^+/Fc in the backward cycle an increase in frequency was observed arising from the stripping of indium(0) and indium–platinum alloys. Between 0.83 V *vs.* Fc^+/Fc in the backward cycle and 0.71 V *vs.* Fc^+/Fc in the forward cycle an increase of frequency is observed due to the anodic decomposition of the ionic liquid. The theoretical amount of indium deposited from −0.77 V *vs.* Fc^+/Fc in the forward cycle to −0.81 V *vs.* Fc^+/Fc in the backward cycle is calculated and compared to the actual mass deposited. A current efficiency of 70% was obtained, leading to the conclusion that

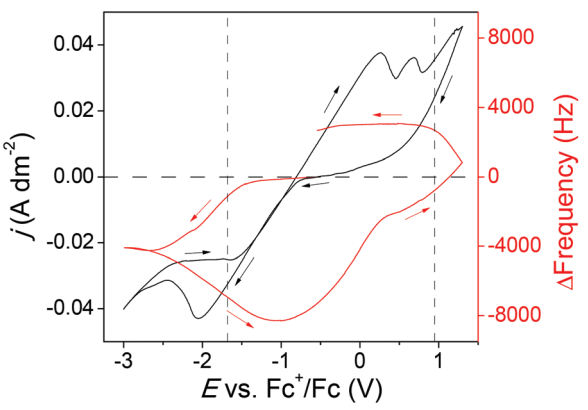

Fig. 7 CV (2nd cycle) of purified Cyphos IL 101 loaded with 50 mM of indium(III) on a Pt electrode at 120 °C (black line, left axis) with EQCM analysis (red line, right axis). Scans were recorded at v_{scan} = 2 mV s^{-1}.

some of the current is used for the reduction of indium(III) to indium(I) and/or the reduction of impurities.

To study the indium electrodeposition mechanism further, a curve of mass/charge (m/z) as a function of the potential was constructed based on Faraday's law and the Sauerbrey equation:

$$\frac{m}{z} = -\frac{FC_f \Delta f}{\Delta Q} \quad (10)$$

where M (g mol^{-1}) is the molar mass of the reducing/oxidizing agent; z is the number of electrons involved in the electrochemical reaction; F = 96 485.34 (C mol^{-1}) is the Faraday constant; ΔQ (C cm^{-2}) is the change in charged consumed during the electrochemical reaction. Eqn (10) can be used to determine m/z as a function of applied potential, which allows to examine changes in reaction mechanisms along a CV. However, when the current in CV goes through zero, experimentally determined m/z values become uncertain. Therefore, these m/z values are removed from the graph. In this paper, we use the absolute negative value of charge change ΔQ in eqn (10), so that m/z has an opposite sign as Δm, *i.e.* negative for deposition and positive for a stripping process.

Fig. 2 shows the CV and EQCM data analyzed for m/z of purified Cyphos IL 101 loaded with 50 mM of indium(III). The value of m/z when indium is being deposited with 100% efficiency, *i.e.*, without any other parallel process on the surface of the electrode is 38.27 g mol^{-1}. From Fig. S10,† it was observed that experimental m/z values obtained during indium reduction start at quite low m/z values. At this stage, indium(III) is mainly reduced to indium(I). Indium(I) is not reduced further to indium(0) and is lost in solution due to disproportionation. As the potential is shifted to more negative values, the reaction rate for the reduction of indium(I) to indium(0) is increased and the m/z values moved toward a value of −38.27 g mol^{-1} as the deposition advanced and stays constant for a while. From −2.47 V *vs.* Fc$^+$/Fc in the forward cycle an −2.45 V *vs.* Fc$^+$/Fc in the backward cycle, decomposition of the ionic liquid takes place, leading to more positive m/z values. The more positive m/z values that are obtained outside of the decomposition potentials of the ionic liquid, but still within the cathodic current range, are due to the simultaneous electrochemical reduction of indium(III) to indium(I) and subsequently disproportionation in combination with the reduction of indium(I) to indium(0).

The stripping of indium(0) and indium–platinum alloys takes place from −0.81 V *vs.* Fc$^+$/Fc to 0.83 V *vs.* Fc$^+$/Fc in the backward cycle. From −0.43 V *vs.* Fc$^+$/Fc to 0.23 V *vs.* Fc$^+$/Fc in the backward cycle, theoretical m/z values more positive than 38.27 g mol^{-1} are obtained indicating that the main electrochemical process taken place is the oxidation of indium(0) to indium(I). Starting from 0.23 V *vs.* Fc$^+$/Fc to 0.83 V *vs.* Fc$^+$/Fc in the backward cycle the theoretical m/z values vary between 38.27 g mol^{-1} and 31.30 g mol^{-1}, illustrating that the simultaneous oxidation of indium(0) to indium(I) followed by a disproportionation reaction of indium(I) is accompanied with oxidation of indium(I) to indium(III). Between 0.83 V *vs.* Fc$^+$/Fc in the backward cycle and 0.71 V *vs.* Fc$^+$/Fc in the forward cycle the anodic decomposition of the ionic liquid takes place accompanied with chlorine gas evolution. Due to the dissolution of Pt in the ionic liquid as platinum chloride the m/z values become uncertain.

This hypothesis is confirmed by using a rotating ring disk electrode (RRDE). Cyclic voltammetry was applied on the disk, while the ring was kept at a potential of 0.5 V *vs.* Fc$^+$/Fc (Fig. 8). During the cathodic scan, indium(III) was reduced to indium(I), but when the indium(I) ions reached the ring, they were re-oxidized to indium(III). In the anodic scan, indium(0) is oxidized to indium(I) and transported to the ring where it is further oxidized to indium(III). Indium(III) is being reduced to indium(0) by a two-step process involving indium(I) and *vice versa* re-oxidized. A current efficiency of 59% was obtained under the assumption that only indium(I) is produced on the disk and that every indium(I) ion produced also reaches the ring.

The two-step deposition reaction of indium(III) to indium(I) and subsequently to indium(0) has already been reported for several chloroindate(III) ionic liquids including Cyphos IL 101.[33,65] Estager *et al.* described a method for establishing the formation of indium(I).[65] By holding the working electrode (platinum) at a potential between that for the reduction to indium(I), and that for electrodeposition of indium(0), electroplating of indium(0) was prevented. The produced indium(I)-containing anions were immediately dispersed in the electrolyte by vigorous stirring. Subsequently, indium(I) disproportionated into indium(0) and indium(III) in the bulk electrolyte leading to the formation of relatively large (>1000 nm), irregular 'chunks' of indium in the case of Cyphos IL 101 due to poor capping agent abilities of the bulky phosphonium cation. In this work, electroreduction of indium(III) to indium(I) on a platinum working electrode was performed at constant

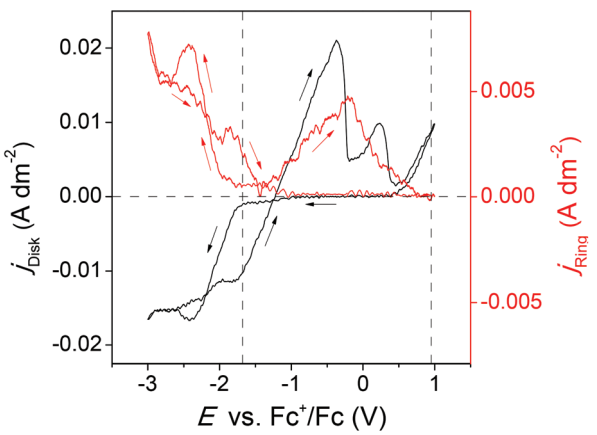

Fig. 8 Disk and ring currents (CV, 2nd cycle) recorded in purified Cyphos IL 101 loaded with 50 mM of indium(III) at 100 rpm at 80 °C. The disk current was generated from the cyclic voltammetry with a scan rate of 2 mV s^{-1}, and the ring was kept at a potential of 0.5 V *vs.* Fc$^+$/Fc. The ring current density data was smoothed by a Savitzky–Golay function with 40 points window size.

potential (E = −1.65 V *vs.* Fc^+/Fc) from purified Cyphos IL 101 with 400 mM indium(III) at 120 °C for 18 h. The experiment was performed in a small porcelain crucible (V = 3 mL) under continuous stirring (1000 rpm) with a magnetic stirring bar. After 18 h, irregular 'chunks' of indium were observed inside the electrolyte and a small amount of indium was found on the platinum electrode (Fig. S11†). The scanning electron microscopy (SEM) images of these 'chunks' are shown in Fig. S12.† The 'chunks' seem to be composed of a great number of smaller pieces sticking together. These 'chunks' did not just fall off the working electrode as a consequence of large amounts of indium being deposited. Indium forms alloys with platinum, so it is expected that a thin film would be formed covering the entire surface. This was not the case, not even when, the surface of the platinum working electrode was abraded with sand paper to improve the adhesion. From these results it can be concluded that indium(I) is indeed involved in the reduction of indium(III).

The morphology of indium deposits on a molybdenum electrode were examined by SEM. The primary concern regarding the indium deposition from chloride medium is the release of chlorine gas at the anode. Fortunately, it has been recently proven that phosphonium ionic liquids are stable in the presence of chlorine gas.[69] Electrodeposition of indium on molybdenum was performed at constant potential (E = −2.00 V *vs.* Fc^+/Fc) from purified Cyphos IL 101 with 400 mM indium(III) at 100 °C, 120 °C, 140 °C, 160 °C and 180 °C for 2 h. The temperature of the electrolyte was measured by placing a thermocouple imbedded in glass in the ionic liquid. The experiments were performed in a small porcelain crucible (V = 3 mL). At all temperatures silvery white deposits were observed on the molybdenum electrode (Fig. 9, 10 and Fig. S13, S14†). From the SEM images, it can be seen that at all temperatures (so even at 100 °C, which is far below the melting point of indium of 156.6 °C) indium deposited as spherical droplets. Below the melting point of indium, coarse indium particles were occasionally observed between the droplets. At temperatures above the melting point of indium, only droplets were observed and some of the spherical particles have a vein-like surface. This is due to solidification of the liquid indium droplets after deposition. If the place of last solidification occurs on the surface, the surface shrinks due to the increase in indium density causing the appearance of vein-like structures. As the temperature increases, so does the packing of droplets. A close packing of droplets, showing droplets on top of other droplets, implying droplet-on-droplet deposition without coalescence was observed starting from 120 °C. Since a continuous indium layer was not obtained, it can be concluded that indium metal does not wet molybdenum. Care had to be taken to avoid removal of the deposits when washing the electrode due to bad adhesion.

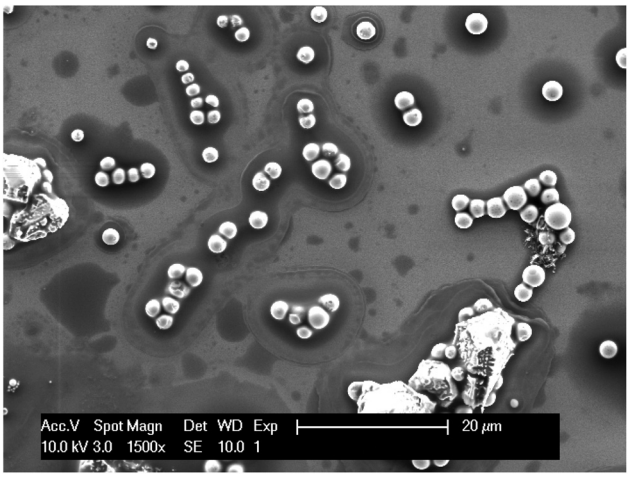

Fig. 9 SEM picture of indium deposited on a molybdenum working electrode at −2.00 V *vs.* Fc^+/Fc at 100 °C for 2 h from purified Cyphos IL 101 loaded with 400 mM of indium(III).

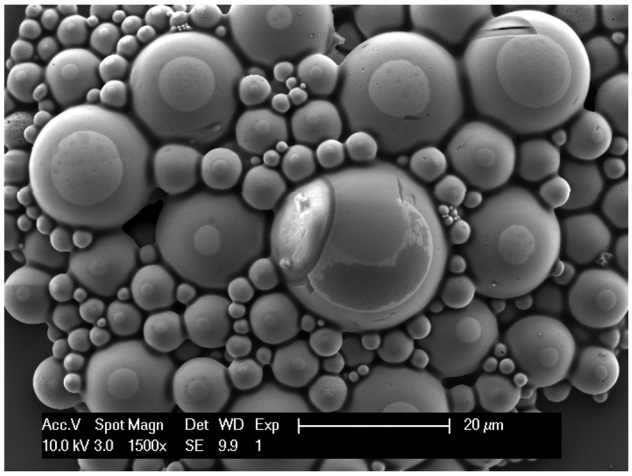

Fig. 10 SEM picture of indium deposited on a molybdenum working electrode at −2.00 V *vs.* Fc^+/Fc at 160 °C for 2 h from purified Cyphos IL 101 loaded with 400 mM of indium(III).

Two possible phenomena can be responsible for the morphologies of the indium that is electrodeposited below the melting point of indium: (1) melting point depression in combination with undercooling or (2) dewetting. Size-dependent melting point depression is an important phenomenon for small particles of nanometer size. These particles have a lower melting point than the bulk material. This is due to the increased influence of the surface atoms as the ratio of surface to bulk atoms increases. As the size of the particles decreases, an increased proportion of atoms occupy surface or interfacial sites. These atoms are more loosely bound than bulk atoms, which facilitates the melting.[70] The size-dependent melting point depression of indium nanoparticles has been studied.[70,71] According to these literature reports, indium particles are liquid at 100 °C when their radius is 3 to 4 nm. If the indium particles being deposited have a radius of 3 to 4 nm, they are deposited in the liquid form. These particles could coalesce without solidifying (undercooling), increasing in size. The presence of coarse indium particles in between the droplets at temperatures below the melting point of indium is an indication that melting point depression could take place. As

can be seen in Fig. 9, all small particles are spherical while the largest particles are non-spherical. This is an indication that the spherical particles are liquid during deposition and consist of undercooled indium. As the particle grow in size by coalescence, the probability for nucleation increases and they become solid and non-spherical.

During solid-state dewetting, thin films, metastable in the as-deposited state, dewet to form isolated islands while the material remains in the solid state. The driving force is minimization of the total energy of the free surfaces of the film and substrate, and of the film-substrate interface.[72] Dewetting can occur *via* surface self-diffusion. Eckert and Drickamer studied the bulk self-diffusion coefficient of indium near the melting point of indium. At 100 °C, the bulk self-diffusion coefficient of indium is approximately 5×10^{-14} m^2 s^{-1}.[73] The surface diffusion coefficient of metals can be 10 to 100 times higher than the bulk diffusion coefficient.[74–76] Considering a surface self-diffusion coefficient equal to, 10 or 100 times larger than the bulk self-diffusion coefficient, the distance over which deposited indium can diffuse to form spherical particles at 100 °C over a time span of 2 h can be estimated from eqn (11) (Table 3):

$$\bar{x} = \sqrt{qDt} = \sqrt{2Dt} \quad (11)$$

in which $\bar{x}$ is the mean displacement, D is the surface self-diffusion coefficient and t is the time. q is a constant depending on the dimensions of the displacement: 2 (1D), 4 (2D), 6 (3D).

The average distance between two single spherical indium particles deposited at 100 °C on the molybdenum electrode is 6.7 μm, so that solid-state dewetting is possible. Liquid state dewetting can explain the droplet deposition above the melting point of indium. The bulk self-diffusion coefficient of indium slightly above the melting point of indium, at 157.30 °C, is around 1×10^{-9} m^2 s^{-1}, a factor 2×10^4 higher than at 100 °C.[73] Considering that the surface self-diffusion coefficient above the melting point of indium is even higher, liquid state dewetting is possible.

Droplet-on-droplet deposition could be explained by the formation of an a surface oxidation layer that is slowly, step by step encapsulating the droplet. Coalescence is prevented as soon as the oxidation layer completely covers the droplet. The In_2O_3 layer is more conducting than indium metal and indium will preferentially be deposited on top of the indium droplets covered with In_2O_3. Although the electrodeposition was executed in an oxygen-free environment (oxygen content glovebox <1 ppm), oxygen can be released by the reduction of oxide-containing impurities or by the reduction of amounts of water still present inside the ionic liquid. Although the reduction of phosphine oxide impurities did not occur, other oxide impurities can be present in Cyphos IL 101.[55] Cyphos IL 101 is synthesized through a quaternization reaction of trihexylphosphine with 1 chlorotetradecane (nucleophilic substitution SN_2).[55,57] When phosphines are oxidized in air, especially trialkyl phosphines, a multitude of oxygen containing byproducts are possible formed.[77,78] Another possibility is that due to the bad wetting of indium metal on molybdenum deposited indium droplets flock together under the influence of capillary forces during drying. In that case, the flocks of indium droplets stacked on top of each other do not originate during deposition but form after deposition.

In order to get more inside in the deposition mechanism and exclude several hypotheses, a dewetting experiment was

Table 3 Mean diffusion distance ($\bar{x}$) of indium atoms at 100 °C during a time span of 2 h as a function of the surface diffusion coefficient

Surface diffusion coefficient (m^2 s^{-1})	$\bar{x}$ (μm)
5×10^{-14}	27
5×10^{-13}	32
5×10^{-12}	100

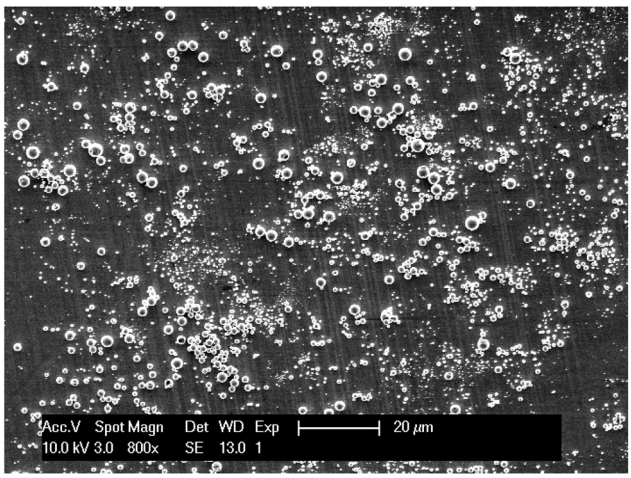

Fig. 11 SEM picture of indium deposited on a molybdenum working electrode at −2.00 V *vs.* Fc^+/Fc at 180 °C for 2 h from purified Cyphos IL 101 loaded with 400 mM of indium(III) after supercritical drying.

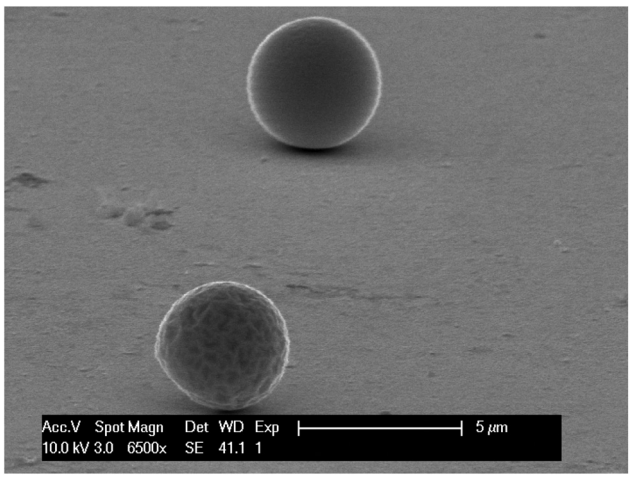

Fig. 12 SEM picture taken at an angle of 70° with the normal of indium deposited on a molybdenum working electrode at −2.00 V *vs.* Fc^+/Fc at 180 °C for 2 h from purified Cyphos IL 101 loaded with 400 mM of indium(III) after supercritical drying.

executed and the indium deposits on molybdenum from Cyphos IL 101 were supercritically dried. For determining dewetting behavior, an uniform indium thin film was deposited on molybdenum from an $InCl_3$ aqueous bath (Fig. S15†). The indium deposit was fused into glass under vacuum and heated in a vacuum oven at 100 °C for 24 h. No significant change in morphology of the deposits was observed before and after heating. The deposits densified due to surface diffusion but showed no signs of dewetting (Fig. S16†). In order to confirm droplet-on-droplet deposition, indium deposited on molybdenum, at −2.00 V *vs.* Fc^+/Fc at 180 °C for 2 h from purified Cyphos IL 101 loaded with 400 mM of indium(III), but this time the deposit was supercritically dried. The SEM pictures show that indium is exclusively being deposited as droplets, some having a vein-like surface (Fig. 11, 12 and Fig. S17†). But instead of a close packing of droplet-on-droplet deposition, individual spherical droplets are observed. The bad wetting of indium metal on molybdenum causes deposited indium droplets to flock together under the influence of capillary forces during normal drying. The contact angle between the indium deposits and the molybdenum working electrode was estimated based on SEM pictures taken at an angle of 70° (Fig. 12). From these figures, the contact angle between the surface and the droplets is estimated to be 175°. In conclusion, the indium particles are being deposited in the liquid form (melting point depression) as individual spheres. These particles coalesce without solidifying (undercooling), increasing in size. As the particle grow in size by coalescence, the probability for nucleation increases and they become solid and non-spherical.

Electrochemical study of zinc and iron on Mo in purified Cyphos IL 101

Zinc and iron are often associated with indium due to their presence in indium-containing ores or by-products.[79–82] Therefore, the capability of Cyphos IL 101 as an electrolyte for the separation of indium and zinc or indium and iron was investigated. CVs of purified Cyphos IL 101 containing 30 mM of zinc(II) or iron(III) chloride were recorded on a Mo WE at 120 °C and 180 °C at a scan rate of 20 mV s^{-1} (Fig. 13). A small reduction peak was observed starting at −1.31 V *vs.* Fc^+/Fc in the forward cycle, probably due to the reduction of a small amount of impurities left in the purified Cyphos IL 101. The corresponding oxidation peak started at 0.32 V *vs.* Fc^+/Fc in the backward cycle and coincided with the anodic decomposition of the ionic liquid. This indicates that co-deposition of zinc with indium can be avoided. In the CV of purified Cyphos IL 101 containing 30 mM of iron(III) a reduction peak starting at 0.09 V *vs.* Fc^+/Fc was observed in the forward cycle. This peak is assigned to the reduction of iron(III) to iron(II) (eqn (12)).[64] The corresponding oxidation peak from iron(II) to iron(III) started at −0.29 V *vs.* Fc^+/Fc in the backward cycle. The additional reduction peak at −2.00 V *vs.* Fc^+/Fc can be attributed to reduction of iron(II) to iron(0) (eqn (13)).[64] The absence of a corresponding oxidation peak can be explained by the comproportionation reaction between iron(0) and iron(III)

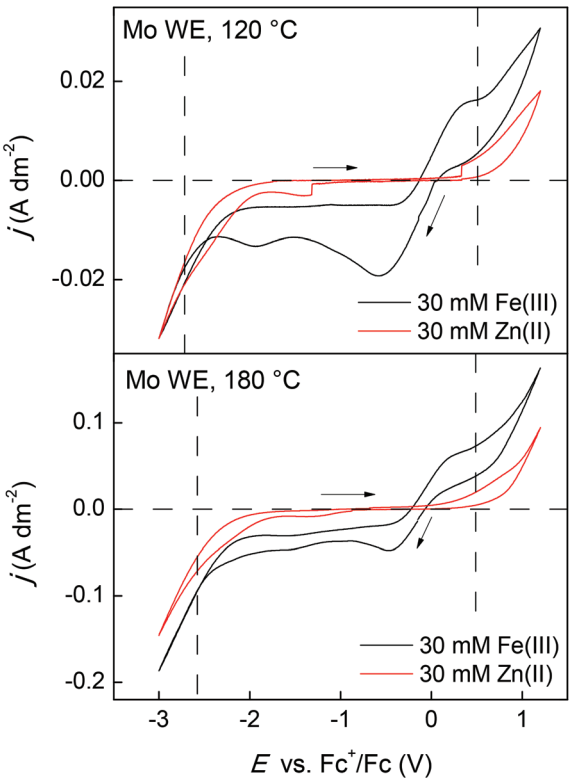

Fig. 13 CVs (2nd cycle) of purified Cyphos IL 101 loaded with 30 mM of zinc(II) or iron(III) on a Mo working electrode (WE) at 120 °C and 180 °C. Scans were recorded at v_{scan} = 20 mV s^{-1}. CVs (1st cycle) are shown in ESI, Fig. S18.†

forming iron(II) (eqn (14)) or by the formation of a passivation layer, $FeCl_2$. $FeCl_3$–Cyphos IL 101 is a Lewis-basic ionic liquid with an excess of Cyphos IL 101 ($FeCl_3$–Cyphos IL 101 mole ratio <0.50) and free chlorides in equilibrium with $[FeCl_4]^-$. Upon dissolution of iron, free chlorides are available making the passivation of iron by $FeCl_2$ very unlikely. The passivation of metals is reported in acidic chlorometallate ionic liquids (MCl_3–ionic liquid mole ratio >0.50).[83–85] In Lewis-acidic ionic liquids the activity of free chlorides is insignificant. Upon dissolution of the metal, the necessary ligands will have to come from the dimeric $[M_2Cl_7]^-$ anions, decreasing the Lewis acidity of the electrolyte at the interface. The solubility of metal chlorides decreases with increasing Lewis acidity of the ionic liquid, forming a passivation layer upon precipitation. The reduction of iron(II) to iron(0) occurred at more positive potentials than the reduction of indium, so that it is difficult to separate iron from indium by electroreduction.

$$Fe^{3+} + e^- \rightleftharpoons Fe^{2+} \quad E_0 = +0.77\ V \tag{12}$$

$$Fe^{2+} + 2e^- \rightleftharpoons Fe \quad E_0 = -0.44\ V \tag{13}$$

$$Fe + 2Fe^{3+} \rightleftharpoons 3Fe^{2+} \tag{14}$$

To investigate if deposition of iron(III) or zinc(II) takes place at the deposition potential of indium, chrono-amperometric experiments were executed at −1.80 V *vs.* Fc^+/Fc and −2.00 V *vs.*

Table 4 Composition of the deposits on a molybdenum working electrode from purified Cyphos IL 101 loaded with 400 mM iron(III), 400 mM zinc(II) and 400 mM indium(III), determined by TXRF

	Chrono-amperometric conditions			
Element	120 °C, 3 h, −1.8 V *vs.* Fc^+/Fc	180 °C, 3 h, −1.8 V *vs.* Fc^+/Fc	120 °C, 2 h, −2.0 V *vs.* Fc^+/Fc	180 °C, 2 h, −2.0 V *vs.* Fc^+/Fc
In	89.9%	25.9%	99.0%	82.8%
Fe	9.8%	73.6%	0.8%	17.0%
Zn	0.3%	0.4%	0.2%	0.2%

Fc^+/Fc. Electrodeposition of iron and zinc on molybdenum was performed at constant potential from purified Cyphos IL 101 loaded with 400 mM iron(III), 400 mM zinc(II) and 400 mM indium(III) at 120 and 180 °C. A 3 h measurement at −1.80 V *vs.* Fc^+/Fc and a 2 h measurement at −2.00 V *vs.* Fc^+/Fc were performed. The experiments were performed in a small porcelain crucible (V = 3 mL). Grey-black deposits were observed on the molybdenum electrodes. Scanning electron microscopy with energy-dispersive X-ray spectroscopy (SEM-EDS) was executed on the deposits. EDS confirmed the presence of iron and indium, but not zinc (Fig. S19–S22†). The composition of the deposits was determined by total reflection X-ray fluorescence spectrometer (TXRF) (Table 4). Very little zinc could be detected. Also, the TXRF results state a strong overestimation of the real concentration of iron in the material deposited at 180 °C. Iron has a limited solubility in indium at 180 °C (<0.3%).[86,87] Indium and iron form two phases. While indium does not form alloys with molybdenum, iron does at temperatures above 700 °C.[88,89] Due to the better wettability between iron and molybdenum, iron will adhere better to molybdenum than indium. Large amounts of indium metal were floating in the electrolyte after deposition not measured by TXRF. Zinc on the other hand can form a liquid alloy with indium at 180 °C and an intermetallic compound ($MoZn_7$) with molybdenum.[90,91]

Hsiu *et al.* investigated the Lewis acidity dependency of the electrochemical window of zinc chloride–1-ethyl-3-methylimidazolium chloride ionic liquids.[92] It was noticed that at a $ZnCl_2$–ionic liquid molar ratio of 1 : 3, the cathodic limit of the electrochemical window corresponds to the reduction of the imidazolium cation rather than the electrodeposition of zinc metal. Zn(II) is present as anionic $ZnCl_4^{2-}$, which is more difficult to reduce than the imidazolium cation. In our system, the $ZnCl_2^-$ ionic liquid ratio is also less than 1 : 3, explaining the absence of zinc(II) deposition, which is due to the presence of Lewis-basic $ZnCl_4^{2-}$ anions.[93] A $ZnCl_2$–ionic liquid ratio above 1 : 3 will probably shift the cathodic limit of the electrochemical window to the deposition of zinc(II) due to the presence of Lewis-acidic zinc(II) species of which the number of chloride that complexed to the zinc is less than four.

Indium speciation in purified Cyphos IL 101

It has been reported in the literature that the speciation of indium in chloroindate(III) ionic liquids based on 1-alkyl-3-methylimidazolium cations ($[C_n mim]^+$, where n = 4 or 8), is dependent of the molar ratio of indium(III) chloride to the organic chloride salt (commonly expressed as the effective mole fraction of 'monomeric' indium(III) chloride, $x InCl_3$.[94–96] $[C_n mim]$-based chloroindate(III) ionic liquids with a composition of $x InCl_3$ = 0.25 have been shown to contain the $[InCl_6]^{3-}$ anion as the major indium species. As more indium(III) chloride was added to the mixture, the major indium species gradually changed to $[InCl_5]^{2-}$ and $[InCl_4]^-$ at $x InCl_3$ = 0.33 and $x InCl_3$ = 0.50, respectively. To verify if the same indium speciation is also present in Cyphos IL 101, EXAFS spectra were recorded of indium(III) chloride dissolved in dry Cyphos IL 101 in three mole fractions $x InCl_3$ = 0.20, 0.25 and 0.33 (Fig. 14). Reference EXAFS spectra of indium(III) chloride dissolved in $[C_8 mim]Cl$ at the same mole fractions $x InCl_3$ = 0.20, 0.25 and 0.33 were recorded for comparison. By fixing the amplitude reduction factor at 0.9, the coordination numbers of all three reference samples matched well with the expected main indium(III) species, namely $[InCl_5]^{2-}$ for $x InCl_3$ = 0.33 and $[InCl_6]^{3-}$ for $x InCl_3$ = 0.25 and 0.20. The same value of the amplitude reduction factor was also used in the fitting of the Cyphos IL 101 samples. The figures with the fitted models of all samples can be found in the ESI (Fig. S23 and S24†). Unexpectedly, the fitted coordination number and the bond distance of all three Cyphos IL 101 samples indicates that the main species in all three Cyphos IL 101 samples is $[InCl_5]^{2-}$ (Table 5). This can also be observed in the Fourier-transform, where the peak of all three Cyphos IL 101 samples lies close to the peak of the $x InCl_3$ = 0.33 reference sample, containing $[InCl_5]^{2-}$ as the main species (Fig. 15). The bond distance increased slightly with decreasing amount of

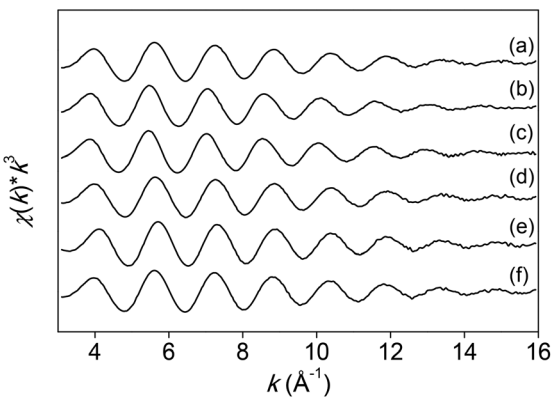

Fig. 14 EXAFS functions of indium(III) chloride dissolved in $[C_8 mim]Cl$: (a) $x InCl_3$ = 0.33, (b) $x InCl_3$ = 0.25 and (e) $x InCl_3$ = 0.20; and in Cyphos IL 101: (d) $x InCl_3$ = 0.33, (e) $x InCl_3$ = 0.25 and (f) $x InCl_3$ = 0.20.

Table 5 Fitting parameters of the EXAFS spectra of indium(III) chloride dissolved in [C_8mim]Cl and Cyphos IL 101 at three mole fractions xInCl$_3$ = 0.33, 0.25 and 0.20. The data of xInCl$_3$ = 0.50 in Cyphos IL 101 were determined in previous work and added for comparison

System	N (–)[b]	R[c] (Å)	$2\sigma^2$[d] (Å^2)	Main species
xInCl$_3$ = 0.33 in [C_8mim]Cl (reference)	5.0(1)	2.432(2)	0.008(1)	$[InCl_5]^{2-}$
xInCl$_3$ = 0.25 in [C_8mim]Cl (reference)	6.0(1)	2.489(2)	0.008(1)	$[InCl_6]^{3-}$
xInCl$_3$ = 0.20 in [C_8mim]Cl (reference)	6.1(1)	2.500(2)	0.008(1)	$[InCl_6]^{3-}$
xInCl$_3$ = 0.33 in Cyphos IL 101	5.1(1)	2.430(2)	0.007(1)	$[InCl_5]^{2-}$
xInCl$_3$ = 0.25 in Cyphos IL 101	5.3(1)	2.441(2)	0.007(1)	$[InCl_5]^{2-}$
xInCl$_3$ = 0.20 in Cyphos IL 101	5.2(1)	2.440(2)	0.007(1)	$[InCl_5]^{2-}$
xInCl$_3$ = 0.50 in Cyphos IL 101[a]	4.0(1)	2.364(2)	0.004(1)	$[InCl_4]^{-}$

[a] Data from previous work.[14] [b] N is the number of coordinating chlorine atoms. [c] R is the interatomic distance. [d] σ^2 is the Debye–Waller factor.

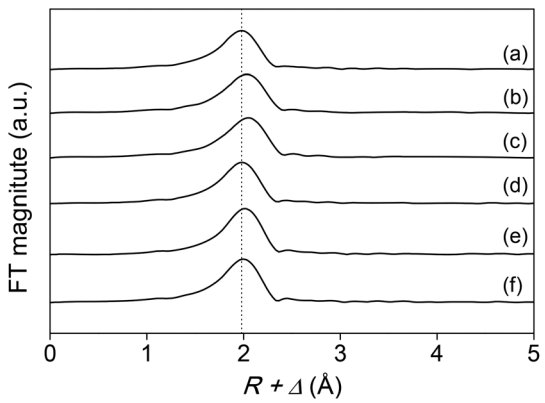

Fig. 15 Fourier-transform of the EXAFS functions of indium(III) chloride dissolved in [C_8mim]Cl: (a) xInCl$_3$ = 0.33, (b) xInCl$_3$ = 0.25 and (e) xInCl$_3$ = 0.20; and in Cyphos IL 101: (d) xInCl$_3$ = 0.33, (e) xInCl$_3$ = 0.25 and (f) xInCl$_3$ = 0.20.

indium(III) chloride dissolved in Cyphos IL 101, from 2.430(2) at xInCl$_3$ = 0.33 to 2.440(2) at xInCl$_3$ = 0.20, thus indicating that a small, but significant and increasing, fraction of $[InCl_6]^{3-}$ is present when lowering the indium(III) concentration. It should be stressed that the indium speciation in dried Cyphos IL 101 clearly differs from that in water-saturated Cyphos IL 101. As reported before, in contrast to the indium speciation in dried Cyphos IL 101, the indium speciation in water-saturated Cyphos IL 101 is independent of the indium concentration, *i.e.* $[InCl_4^-]$.[14]

An indium(III) chloride concentration between 10 and 400 mM in Cyphos IL 101 was used in the previous experiments corresponding to a composition between xInCl$_3$ = 0.19 and 0.006, respectively. Therefore, based on the EXAFS results it can be concluded that the major indium(III) species in solution with composition xInCl$_3$ = 0.19 corresponds to the $[InCl_5]^{3-}$ complex. As the indium(III) chloride concentrations decreases, it is expected that an increasing fraction of $[InCl_6]^{3-}$ will be present. However, the data are inconclusive with respect to the major indium(III) species at very low indium(III) chloride concentrations. It is unclear whether $[InCl_6]^{3-}$ will become the major indium(III) species in solution with ever decreasing indium(III) chloride concentration. As a consequence, the calculated diffusion coefficient $(7.5 \pm 0.1) \times 10^{-12}$ m^2 s^{-1} at 120 °C (ESI†) could belong to either the $[InCl_5]^{2-}$ or the $[InCl_6]^{3-}$ anion in Cyphos IL 101 (10 mM In, 120 °C).

Conclusions

The electrochemical behavior of indium in the ionic liquid trihexyl(tetradecyl)phosphonium chloride (Cyphos IL 101) was investigated at 120 °C and 180 °C. Commercial Cyphos IL 101 had to be purified due to interference of impurities in the electrochemical measurements. The electrochemical deposition of indium followed a two-step process, involving the reduction of indium(III) to indium(I), followed by the reduction of indium (I) to indium(0). Indium was deposited at temperatures ranging from 100 to 180 °C. The morphology of the indium deposits was examined by SEM. At all temperatures, droplet-like deposits of indium were observed. The formation of droplets has a two-fold origin: melting-point depression of very small primary indium particles in combination with undercooling. The capability of the electrolyte to eliminate iron(III) and zinc(II) electrochemically was tested by adding indium(III) together with zinc (II) and iron(III) to Cyphos IL 101. Zinc(II) was not co-deposited with indium(III) because the formation of the Lewis-basic $ZnCl_4^{2-}$ anions shifts the deposition potential outside of the cathodic limit of the phosphonium cation. Iron(III) could not be separated from indium(III) in this way. A diffusion coefficient of $(7.5 \pm 0.1) \times 10^{-12}$ m^2 s^{-1} was obtained for the chloroindate(III) anion in Cyphos IL 101 (10 mM In, 120 °C).

Conflicts of interest

There are no conflicts to declare.

Acknowledgements

This research was supported by the Flemish Institute for the Promotion of Innovation by Science and Technology (IWT Vlaanderen) *via* a Baekeland PhD fellowship to Clio Deferm (IWT 130305) and by the Umicore Group Research & Development. The research leading to these results also received funding from the European Research Council (ERC) under the European Union's Horizon 2020 Research and

Innovation Programme: Grant Agreement 694078—Solvometallurgy for critical metals (SOLCRIMET). Joop van Deursen made and designed the EQCM cell. The authors also wish to thank FWO for funding the EXAFS measurements, DUBBLE staff for their support, Wouter Monnens for his assistance during measuring shifts at the beamline, Alina Arslanova for providing Matlab support and Frederik Ceyssens for the supercritical drying experiments.

Notes and references

1 N. Felix, in *Ullmann's Encyclopedia of Industrial Chemistry*, ed. F. Ullmann, Wiley-VCH, Weinheim, 2012, vol. 19, pp. 65–74.
2 U. Scwarz-Schampera and P. M. Herzig, *Indium: Geology, Mineralogy, and Economics*, Springer Verlag, New York, 2002.
3 D. Kiriya, M. Zheng, R. Kapadia, J. Zhang, M. Hettick, Z. Yu, K. Takei, H.-H. H. Wang, P. Lobaccaro and A. Javey, *J. Appl. Phys.*, 2012, **112**, 123102.
4 K. Tachibana, T. Someya and Y. Arakawa, *Appl. Phys. Lett.*, 1999, **74**, 383–385.
5 K. H. Kim, K. H. Yoon, J. H. Yun and B. T. Ahn, *Electrochem. Solid-State Lett.*, 2006, **9**, A382–A385.
6 D. A. Browne, E. C. Young, J. R. Lang, C. A. Hurni and J. S. Speck, *J. Vac. Sci. Technol., A*, 2012, **30**, 041513.
7 R. N. Bhattacharya, *Sol. Energy Mater. Sol. Cells*, 2013, **113**, 96–99.
8 I. M. Dharmadasa and J. Haigh, *J. Electrochem. Soc.*, 2006, **153**, G47–G52.
9 A. M. Alfantazi and R. R. Moskalyk, *Miner. Eng.*, 2003, **16**, 687–694.
10 W.-S. Chen, *Int. J. Appl. Ceram. Technol.*, 2016, **13**, 274–279.
11 M.-S. Lee and K.-Y. Sohn, *J. Mater. Sci.*, 2003, **38**, 4843–4848.
12 F. C. Walsh and D. R. Gabe, *Surf. Technol.*, 1979, **8**, 87–99.
13 C. Deferm, M. Van de Voorde, J. Luyten, H. Oosterhof, J. Fransaer and K. Binnemans, *Green Chem.*, 2016, **18**, 4116–4127.
14 C. Deferm, B. Onghena, T. Vander Hoogerstraete, D. Banerjee, J. Luyten, H. Oosterhof, J. Fransaer and K. Binnemans, *Dalton Trans.*, 2017, **46**, 4412–4421.
15 R. Piercy and N. A. Hampson, *J. Appl. Electrochem.*, 1975, **5**, 1–15.
16 J. C. Malaquias, M. Steichen, M. Thomassey and P. J. Dale, *Electrochim. Acta*, 2013, **103**, 15–22.
17 Z. Liu, G. Pulletikurthi, A. Lahiri, T. Cui and F. Endres, *Dalton Trans.*, 2016, **45**, 8089–8098.
18 T. Jiang, M. J. Chollier Brym, G. Dubé, A. Lasia and G. M. Brisard, *Surf. Coat. Technol.*, 2006, **201**, 1–9.
19 T. Jiang, M. J. Chollier Brym, G. Dubé, A. Lasia and G. M. Brisard, *Surf. Coat. Technol.*, 2006, **201**, 10–18.
20 F. Endres, *ChemPhysChem*, 2002, **3**, 144–154.
21 P. Giridhar, S. Zein El Abedin and F. Endres, *Electrochim. Acta*, 2012, **70**, 210–214.
22 G. R. Stafford and C. L. Hussey, in *Advances in Electrochemical Science and Engineering*, ed. R. C. Alkire and D. M. Kolb, Wiley-VCH, Weinheim, 2001, vol. 7, pp. 275–347.
23 T. Schubert, S. Zein, E. Abedin, A. P. Abbott, K. J. McKenzie, K. S. Ryder and F. Endres, in *Electrodeposition from Ionic Liquids*, ed. F. Endres, D. MacFarlane and A. P. Abbott, Wiley-VCH, Weinheim, 2008, pp. 83–124.
24 J. S.-Y. Liu and I.-W. Sun, *J. Electrochem. Soc.*, 1997, **144**, 140–145.
25 T. Beyersdorff, T. J. S. Schubert, U. Welz-Biermann, W. Pitner, A. P. Abbott, K. J. McKenzie and K. S. Ryder, in *Electrodeposition from Ionic Liquids*, ed. F. Endres, D. MacFarlane and A. P. Abbott, Wiley-VCH, Weinheim, 2008, pp. 15–46.
26 E. L. Smith, A. P. Abbott and K. S. Ryder, *Chem. Rev.*, 2014, **114**, 11060–11082.
27 M. F. Rahman, R. Bernasconi and L. Magagnin, *J. Optoelectron. Adv. Mater.*, 2015, **17**, 568–572.
28 M.-H. Yang, M.-C. Yang and I.-W. Sun, *J. Electrochem. Soc.*, 2003, **150**, C544–C548.
29 M.-H. Yang and I.-W. Sun, *J. Chin. Chem. Soc.*, 2004, **51**, 253–260.
30 S.-I. Hsiu, C.-C. Tai and I.-W. Sun, *Electrochim. Acta*, 2006, **51**, 2607–2613.
31 S. Zein El Abedin, A. Y. Saad, H. K. Farag, N. Borisenko, Q. X. Liu and F. Endres, *Electrochim. Acta*, 2007, **52**, 2746–2754.
32 Y. Traorea, S. Legeai, S. Diliberto, G. Arrachart, S. Pellet-Rostaing and M. Draye, *Electrochim. Acta*, 2011, **58**, 532–540.
33 M. K. Carpenter and M. W. Verbrugge, *J. Mater. Res.*, 1994, **9**, 2584–2591.
34 Y.-C. Liu, Y.-C. Chen, Y.-T. Hsieh and I.-W. Sun, *J. Phys. Chem. C*, 2017, **121**, 8907–8913.
35 J. Zhang, M. An, A. Liu, S. Ji, Y. Lian and X. Ren, *J. Electrochem. Soc.*, 2016, **163**, D707–D709.
36 M. Matsumiya, M. Sumi, Y. Uchino and I. Yanagi, *Sep. Purif. Technol.*, 2018, **201**, 25–29.
37 A. A. C. Alcanfor, L. P. M. dos Santos, D. F. Dias, A. N. Correia and P. de Lima-Neto, *Electrochim. Acta*, 2017, **235**, 553–560.
38 J. C. Malaquias, M. Steichen and P. J. Dale, *Electrochim. Acta*, 2015, **151**, 150–156.
39 H. A. Øye, N. Mason, R. D. Peterson, N. E. Richards, E. L. Rooy, F. J. Stevens McFadden, R. D. Zabreznik, F. S. Williams and R. B. Wagstaff, *JOM*, 1999, **51**, 29–42.
40 M. Gibilaro, S. Bolmont, L. Massot, L. Latapie and P. Chamelot, *J. Electroanal. Chem.*, 2014, **726**, 84–90.
41 G.-Y. Kim, T.-J. Kim, S.-H. Kim and S. Paek, *J. Radioanal. Nucl. Chem.*, 2014, **300**, 1261–1265.
42 G.-Y. Kim, J. Shin, S.-H. Kim, D.-H. Ahn and S. Paek, *J. Radioanal. Nucl. Chem.*, 2016, **307**, 1551–1557.
43 C. S. Wang, Y. Liu, H. He, F. X. Gao, L. S. Liu, S. W. Chang, J. H. Guo, L. Chang, R. X. Li and Y. G. Ouyang, *J. Radioanal. Nucl. Chem.*, 2013, **298**, 581–586.
44 M. V. Ginatta, *JOM*, 2000, **52**, 18–20.
45 Y. Kado, A. Kishimoto and T. Uda, *J. Electrochem. Soc.*, 2013, **160**, E139–E142.

46 B. K. Sharma, *Electro Chemistry*, Krishna Prakashan Media, Meerut, 1985.
47 J. Bouteillon, M. Jafarian, J. C. Poignet and A. Heydet, *J. Electrochem. Soc.*, 1992, **139**, 1–5.
48 Y. Castrillejo, M. A. Garcia, E. Barrado, P. Pasquier and G. S. Picard, *Electrochim. Acta*, 1995, **40**, 2731–2738.
49 Y. Castrillejo, M. R. Bermejo, A. M. Martinez, C. Abejón, S. Delpech and G. S. Picard, *J. Appl. Electrochem.*, 1999, **29**, 65–73.
50 B. Qin, P. Cui, A. M. Martinez, R. E. Aune and G. M. Haarberg, *ECS Trans.*, 2014, **64**, 249–255.
51 E. I. Rogers, B. Šljukić, C. Hardacre and R. G. Compton, *J. Chem. Eng. Data*, 2009, **54**, 2049–2053.
52 J. Park, Y. Jung, P. Kusumah, J. Lee, K. Kwon and C. K. Lee, *Int. J. Mol. Sci.*, 2014, **15**, 15320–15343.
53 M. C. Buzzeo, R. G. Evans and R. G. Compton, *ChemPhysChem*, 2004, **5**, 1106–1120.
54 M. Hayyan, F. S. Mjalli, M. A. Hashim, I. M. AlNashef and T. X. Mei, *J. Ind. Eng. Chem.*, 2013, **19**, 106–112.
55 C. Deferm, A. Van den Bossche, J. Luyten, H. Oosterhof, J. Fransaer and K. Binnemans, *Phys. Chem. Chem. Phys.*, 2018, **20**, 2444–2456.
56 C. J. Bradaric, A. Downard, C. Kennedy, A. J. Robertson and Y. Zhou, *Green Chem.*, 2003, **5**, 143–152.
57 K. J. Fraser and D. R. MacFarlane, *Aust. J. Chem.*, 2009, **62**, 309–321.
58 CYTEC, CYPHOS IL 101 Data sheet, 2005.
59 M. C. Buzzeo, R. G. Evans and R. G. Compton, *ChemPhysChem*, 2004, **5**, 1106–1120.
60 R. A. Mantz, in *Ionic Liquids in Synthesis*, ed. P. Wasserscheid and T. Welton, Wiley-VCH, Weinheim, 2008, vol. 1, pp. 141–174.
61 A. P. Abbott, F. Endres and D. R. MacFarlane, in *Electrodeposition from Ionic Liquids*, ed. A. P. Abbott, F. Endres and D. R. MacFarlane, Wiley-VCH, Weinheim, 2017, 2th edn, pp. 457–468.
62 E. Dziwinski and J. Szymanowski, *Solvent Extr. Ion Exch.*, 1998, **16**, 1515–1525.
63 J. Vaughan and D. Dreisinger, *J. Electrochem. Soc.*, 2008, **155**, D68–D72.
64 P. Vanýsek, in *CRC Handbook of Chemistry and Physics*, ed. W. M. Haynes, CRC Press, Boca Raton, 92th edn, 2011, pp. 5-80–5-89.
65 J. Estager, P. Nockemann, K. R. Seddon, G. Srinivasan and M. Swadźba-Kwaśny, *ChemSusChem*, 2012, **5**, 117–124.
66 H. Okamoto, *J. Phase Equilib. Diffus.*, 2005, **26**, 399.
67 W. G. Moffatt, *The Handbook of Binary Phase Diagrams*, General Electric Company, Schenectady, 1978, vol. 4, p. 3/82.
68 A. J. Bard and L. R. Faulkner, *Electrochemical Methods, Fundamentals and Applications*, John Wiley & Sons, New York, 2001, ch. 9, p. 339.
69 X. Li, A. Van den Bossche, T. Vander Hoogerstraete and K. Binnemans, *Chem. Commun.*, 2018, **54**, 475–478.
70 M. Zhang, M. Yu. Efremov, F. Schiettekatte, E. A. Olson, A. T. Kwan, S. L. Lai, T. Wisleder, J. E. Greene and L. H. Allen, *Phys. Rev. B: Condens. Matter Mater. Phys.*, 2000, **62**, 10548–10557.
71 C. J. Coombes, *J. Phys. F: Met. Phys.*, 1972, **2**, 441–449.
72 C. V. Thompson, *Annu. Rev. Mater. Res.*, 2012, **42**, 399–434.
73 R. E. Eckert and H. G. Drickamer, *J. Chem. Phys.*, 1952, **20**, 13–17.
74 H. G. Bowden and R. W. Balluffi, *Philos. Mag.*, 1996, **19**, 1001–1014.
75 D. B. Butrymowicz, J. R. Manning and M. E. Read, *J. Phys. Chem. Ref. Data*, 1973, **2**, 643–655.
76 G. B. Sushko, A. V. Verkhovtsev, A. V. Yakubovich, S. Schramm and A. V. Solov'yov, *J. Phys. Chem. A*, 2014, **118**, 6685–6691.
77 C. R. Hilliard, N. Bhuvanesh, J. A. Gladysz and J. Blümel, *Dalton Trans.*, 2012, **41**, 1742–1754.
78 S. A. Buckler, *J. Am. Chem. Soc.*, 1962, **84**, 3093–3097.
79 J.-J. Ke, R.-Y. Qiu and C.-Y. Chen, *Hydrometallurgy*, 1984, **12**, 217–224.
80 X.-H. Li, Y.-J. Zhang, Q.-L. Qin, L. Yang and Y.-S. Wei, *Trans. Nonferrous Met. Soc. China*, 2010, **20**, s141–s145.
81 H. N. Kang, J.-Y. Lee and J.-Y. Kim, *Hydrometallurgy*, 2011, **110**, 120–127.
82 J. Ruan, Y. Guo and Q. Qiao, *Procedia Environ. Sci.*, 2012, **16**, 545–551.
83 D. Xue, Y. Yang and G. Ling, *Green Energy Environ.*, 2017, **2**, 412–418.
84 Q.-F. Pei, Y.-X. Hua, C.-Y. Xu, Q.-B. Zhang, Y. Li, J.-J. Ru and K. Gong, *Acta Phys.–Chim. Sin.*, 2013, **29**, 946–952.
85 C. Wang, A. Creuziger, G. Stafford and C. L. Hussey, *J. Electrochem. Soc.*, 2016, **163**, H1186–H1194.
86 O. K. Goldbeck, in *IRON—Binary Phase Diagrams*, Springer, Berlin, 1982, p. 53.
87 H. Okamoto, *Bull. Alloy Phase Diagrams*, 1990, **11**, 143–146.
88 B. Predel, in *Hg-Ho – La-Zr. Landolt-Börnstein - Group IV Physical Chemistry (Numerical Data and Functional Relationships in Science and Technology)*, ed. O. Madelung, Springer, Berlin, 1997, vol. 5G, p. 1.
89 R. Morales, D. Sichen, S. Seetharaman and I. Arvanitidis, *Metall. Mater. Trans. B*, 2002, **33**, 589–594.
90 J. Pstruś, Z. Moser and W. Gąsior, *Appl. Surf. Sci.*, 2011, **257**, 3867–3871.
91 B. Predel, in *Li-Mg – Nd-Zr. Landolt-Börnstein - Group IV Physical Chemistry (Numerical Data and Functional Relationships in Science and Technology)*, ed. O. Madelung, Springer, Berlin, 1997, vol. 5G, pp. 1–2.
92 S.-I. Hsiu, J.-F. Huang, I.-W. Sun, C.-H. Yuan and J. Shiea, *Electrochim. Acta*, 2002, **47**, 4367–4372.
93 J. Estager, P. Nockemann, K. R. Seddon, M. Swadźba-Kwaśny and S. Tyrrell, *Inorg. Chem.*, 2011, **50**, 5258–5271.
94 J. Estager, A. A. Oliferenko, K. R. Seddon and M. Swadźba-Kwaśny, *Dalton Trans.*, 2010, **39**, 11375–11382.
95 D. C. Apperley, C. Hardacre, P. Licence, R. W. Murphy, N. V. Plechkova, K. R. Seddon, G. Srinivasan, M. Swadźba-Kwaśny and I. J. Villar-Garciac, *Dalton Trans.*, 2010, **39**, 8679–8687.
96 C. Hardacre, R. Murphy, K. R. Seddon, G. Srinivasan and M. Swadźba-Kwaśny, *Aust. J. Chem.*, 2010, **63**, 845–848.

